RECENT RESULTS FROM ZAP ENERGY'S SHEARED-FLOW-STABILIZED Z PINCH EXPERIMENTAL PLATFORMS

B. LEVITT, D. A. SUTHERLAND, E. T. MEIER, J. R. BARHYDT, C. LIEKHUS-SCHMALTZ, U. SHUMLAK
Zap Energy
Seattle, USA
Email: blevitt@zap.energy

G. A. WURDEN
Los Alamos National Laboratory
Los Alamos, NM

C. GOYON, A. E. YOUMANS, D. P. HIGGINSON
Lawrence Livermore National Laboratory
Livermore, CA

S. C. BOTT-SUZUKI, J. T. BANASEK
University of California San Diego
La Jolla, CA

Abstract

Sustained fusion reactions have been measured in a $T_e, T_i > 2$ keV deuterium Z-pinch plasma which is stabilized by radially sheared axial flows. Thomson scattering results from the FuZE device [1, 2] show the onset of high plasma temperature is coincident with a stabilized quiescent period and neutron production. Measurements from neutron detectors demonstrated that 2.45 MeV neutrons were emitted from an extended portion of the 50-cm pinch assembly region, the length of which can be controlled by the specifics of the deuterium gas injection [3]. Additionally, neutron spectroscopic measurements indicate a thermonuclear production process with limited beam-target effects [4]. A new experimental platform, FuZE–Q[5, 6], is now online, and for the first time couples a SFS Z pinch to a megaJoule class capacitor power bank, extending the operational regime and plasma performance of these devices. The neutron yield scaling from recent FuZE-Q campaigns shows strong dependence on pinch current in both model and experiment, agreeing with a simple scaling model consistent with $\propto I^{11}$ [7, 6]. These promising results indicate that a sheared-flow-stabilized (SFS) Z pinch could scale to an extremely compact, economical fusion power plant. Investigations of the effect of plasma wall interactions show that the SFS Z pinch concept may be relatively robust to the effects of impurity contamination, with specific design points capable of accessing $Q_{sci} \geq 10$ with $Z_{eff} \approx 4$. This is a significant finding for this configuration, which features direct contact of the high β fusion-generating plasma with plasma facing material surfaces.

1. INTRODUCTION

In a static Z-pinch equilibrium, an axial pinch current radially confines plasma pressure such that increasing the current results in higher densities and temperatures. While virulent pressure-driven instabilities are known to quickly destroy the traditional Z-pinch equilibrium, theory showed that introducing a sheared axial flow stabilizes the plasma [8]. Closely coupled with computational studies, a series of Z-pinch experiments at the University of Washington [8, 9, 10, 11] tested the theory of sheared-flow stabilization, showing the effect of velocity shear on instability growth, as seen qualitatively in Fig. 1. Experimental measurements of the plasma equilibrium and stability confirmed that in the presence of a sufficiently large flow-shear, gross Z-pinch instabilities were mitigated, and radial force balance was achieved [7]. Both the image from the V-UV fast camera and the modeled ion density profile in Fig. 1 show similar structures, which are indicative of sheared instability structures associated with delayed mode growth and limitations to radial fuel losses. In various generations of SFS Z-pinch plasmas, discharges of 50, 100, and 126–cm lengths were held stable for durations much longer than predicted for a static plasma, i.e. thousands of mode growth times [7].

This paper summarizes recent studies on two SFS Z-pinch devices at Zap Energy: the FuZE and FuZE-Q platforms. FuZE was built and operated at the University of Washington before moving to a Zap Energy facility in 2020, while FuZE-Q was designed, built, commissioned and is currently operated fully by Zap Energy staff. The two devices are fully operational, each with separate capacitor power banks and a complete plasma measurement diagnostic suite for science evaluation. The FuZE device is driven by a lower stored energy bank, ∼80 kJ, and

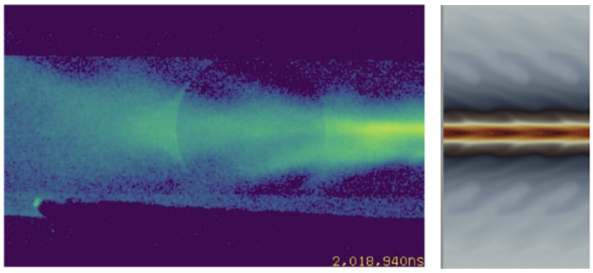

FIG. 1. Left: a false-color image from a visible light fast camera showing a sheared $m = 0$ sausage mode in a FuZE discharge. Right: ion density profiles from nonlinear five-moment-two-fluid simulations starting from FuZE-like equilibria, showing that with a parabolic sheared flow with an edge speed of half the Alfven speed the mode growth is delayed, instability structures are sheared and limited in radial extent by the shear, and a relaxed near-equilibrium state is established [12].

focuses on core science studies, device concept development, and diagnostic testing, while FuZE-Q has a much larger current driver, $\sim$1 MJ, for fusion performance optimization. Updates on selected recent results from both devices are covered in this paper along with a look forward to assess the robustness of the SFS Z-pinch concept to impurity content for future power plant relevant scenarios. Section 2 covers recent experimental results, beginning with a description of our diagnostic capabilities; presenting Thomson Scattering and soft xuv measurements of T_e from the FuZE device; and covering descriptions of the pinch axial extent, as measured by V-UV fast cameras as well as an axial arrays of neutron detectors. Section 3 briefly describes performance scaling SFS Z pinches to relevant gain scenarios via adiabatic compression and presents supporting results from both devices. Section 4 further outlines how performance scaling may be effected by inclusion of impurity content, which is a key risk for this concept. Finally, we conclude in Sec. 5.

2. RECENT PROGRESS

2.1. FuZE-Q Diagnostic Suite

Based on these early studies and the strong indications of performance scaling, Zap Energy is developing the SFS Z pinch for fusion energy applications. The efforts to achieve the necessary performance improvements are aided by a suite of advanced diagnostics, summarized in Fig. 2: an array of 94 in-vacuum surface magnetic probes spaced axially and azimuthally are embedded into the outer electrode to measure the field and current distribution of the plasma at the wall; a suite of fast plastic scintillating detectors, or SPMTs, (labeled “n” in the figure) measure the temporal and spatial neutron source as well as neutron energy spectroscopy [3, 4]; a series of neutron activation detectors (Lanthanum Bromide, Arsenic, Rhodium) measure total neutron yield (labeled “Y_n”); line-integrated density is measured along individual HeNe 633 nm interferometry chords at various locations throughout the device (labeled “HeNe IF”); a Thomson scattering (labeled “TS”) system measures electron temperature and density at 17 locations across the device at a fixed axial location [1]; ion temperature, density and velocity is measured from Doppler broadening of impurity emission lines (labeled “IDS”); two dimensional density imaging is enabled via digital holographic interferometry (labeled “DHI”); an extreme ultraviolet spectrometer measures emission spectra in the 5–40 nm wavelength range for impurity identification, radiative power studies as well as plasma temperature and density measurements (labeled “EUV”); V-UV fast camera imaging is available at various view-ports along the device (labeled “Fast cam”) as well as a high frame-rate X-ray imaging detector (labeled “X-ray cam”). Finally, *circuit* diagnostics consist of the voltage measured across the electrodes (labeled “V_{gap}”) as well as the total plasma current across the electrodes as measured by a Rogowski coil, (labeled “I_p”).

Various other diagnostic systems are under development, including a polarimeter for measuring the Faraday rotation of internal magnetic fields; a Zeeman spectroscopy system, also for internal field detection; and an x-ray crystal spectrometer for measuring properties of higher energy impurity lines.

2.2. Recent Experimental Results

As Zap has grown into a larger company, we are now able to field two fusion platforms, each producing significant science output from their own suite of measurements. At an earlier phase in the company’s development, external collaborations funded by ARPA-E with national laboratory teams significantly accelerated our diagnostic capabilities. Fruitful examples of these interactions were a collaboration with Lawrence Livermore National Laboratory (LLNL) to field the SPMT detectors discussed above; a collaboration with Los Alamos National Laboratory (LANL) to field soft x-ray diagnostics as well as plasma fast imaging capabilities; an ongoing collaboration with University of Nevada Reno (UNR) to develop the EUV diagnostic discussed above; and finally a collaboration with Lawrence Livermore National Laboratory (LLNL) and UC San Diego to field a Thomson scattering diagnostic for measurements of T_e and n_e.

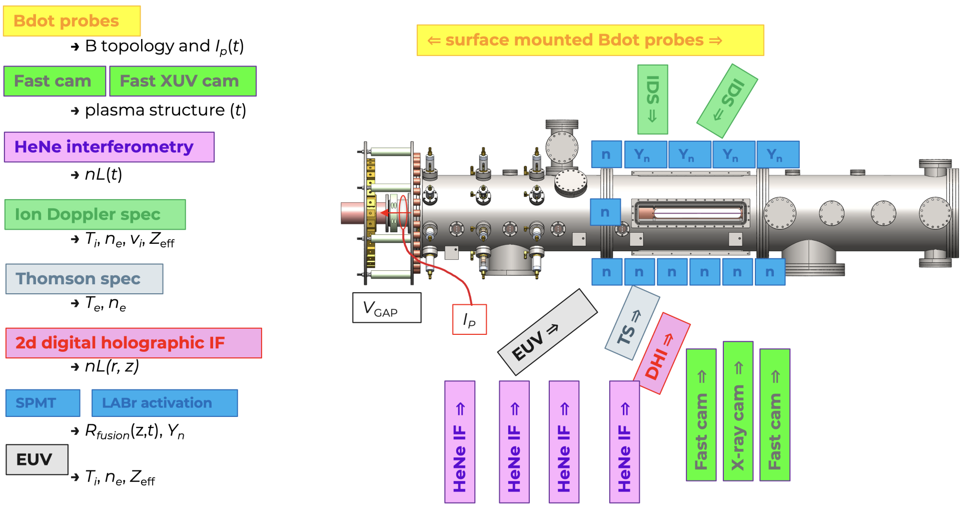

FIG. 2. The FuZE-Q diagnostic suite, along with relevant measured parameters listed at left. See a more detailed description in the text. I_p is plasma current; nL is the line-integrated density; T_i is ion temperature; v_i is ion velocity; n_e is electron density; T_i is electron temperature; Z_{eff} is the plasma impurity fraction; R_{fusion} is the fusion neutron production rate; Y_n is the neutron yield.

Recent campaigns focused on performing multi-point, time resolved Thomson scattering measurements [1] on the FuZE device. Electron temperatures in excess of 2 keV [2] were achieved simultaneous with neutron production and peak current, as shown in Fig. 3. This figure presents a slightly lower temperature shot with a $\approx$ 6 mm radial profile peaked at $\approx$ 1.4 keV. These results confirm earlier inferred T_e measurements from soft x-ray measurements undertaken with LANL collaborators, Fig. 4. The inferred T_e plotted in red results from taking the ratios of the transmission through two different filter materials and applying an assumption of a Maxwellian temperature distribution. This time resolved result provides a useful comparison to the single-time TS measurements, though the interpretation of the inferred T_e from the soft x-ray diagnostic can be challenging due to contaminating x-rays generated from plasma wall interactions.

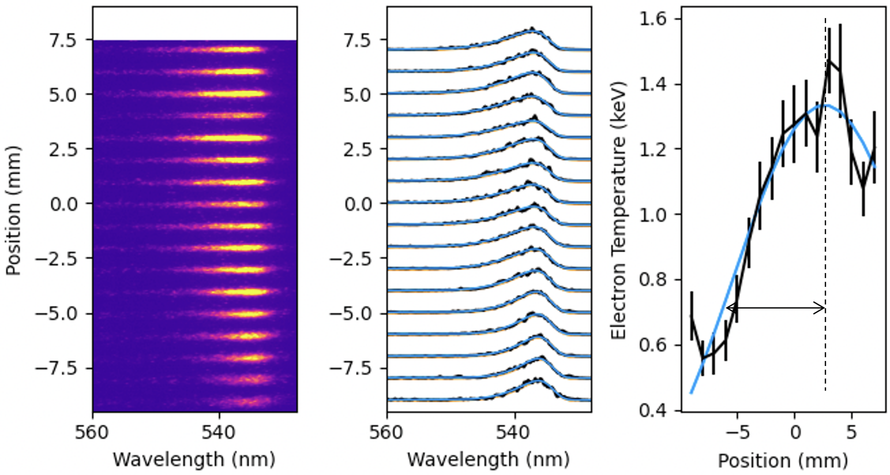

FIG. 3. Raw Thomson data (left column) and fits (middle column) for 17 fibers from a FuZE pulse. Increased broadening of the spectra represent higher plasma temperatures. The reconstruction of the radial profile is shown in the right column, from which we deduce a plasma temperature profile with a radius on the order of 6 mm, as indicated in the figure.

Another Zap Energy collaboration with LLNL deployed an array of neutron scintillators (top right panel of Fig. 5) used to measure the spatial and temporal details of the fusion production, calibrated neutron yields, and neutron energy spectroscopy, which can differentiate thermonuclear versus beam target contributions to the fusion yield. The right bottom panel of Fig. 5 shows that an extended source of $\approx$ 30 cm provides the best fit to the neutron measurements[3]. The left panel of the figure also shows a visible light image of the plasma consistent with this

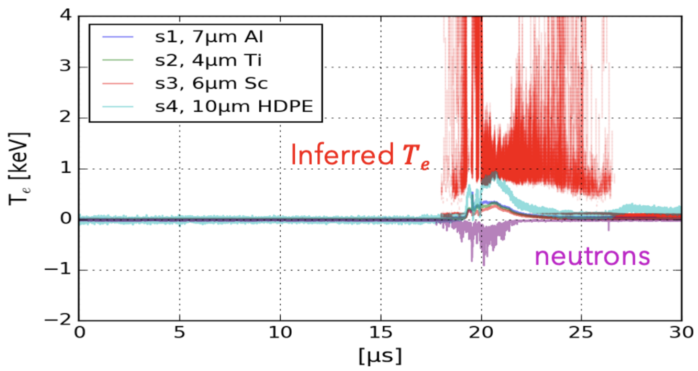

FIG. 4. A time resolved measurement of inferred T_e based on transmission of soft x-rays through a series of filtered diodes. The inferred T_e agrees well with observations from TS. The temporal behavior also agrees well with multi-shot reconstructions from TS data [2]. Lower limits on T_e set by this ratio method are more reliable than the upper limits, which can become unphysical as the transmission through the filter pairs increases at higher photon energies.

axial extent, taken by an optical fast framing camera provided by our LANL collaborators. (This frame is taken at an earlier time in the discharge than when neutron emission is peaked, when we typically observe maximum light emission in the V-UV range.) A further significant result from the SPMT detectors is discussed in Section 3, which addresses the observed and expected scaling of neutron yield as a function of the SFS Z pinch current.

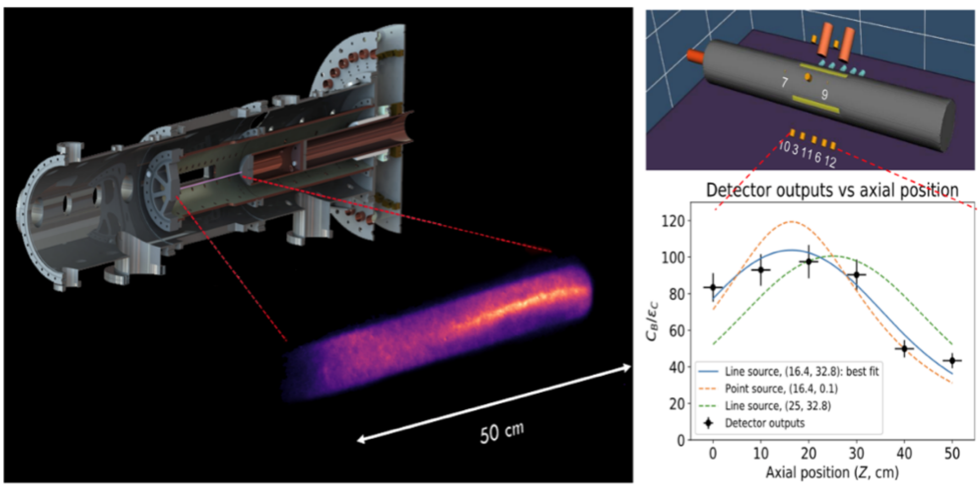

FIG. 5. Left: A visible light image of the FuZE Z pinch. Right panels: schematic of the axial SPMT array (top) and the resulting axial profile measurements (bottom).

3. SCALING VIA ADIABATIC COMPRESSION

A method of assessing the fusion performance of the experimental SFS Z-pinch platforms is against the projected scaling as pinch current is increased[13]. The Bennett relation[14], applicable to any Z pinch with radial force balance between magnetic ($\mathbf{j} \times \mathbf{B}$) and thermal ($\nabla p$) forces, gives the temperature scaling, $T \propto I^2$, where I refers to the current in the pinch, as distinct from I_p, which we designate as total plasma current in the device. Assuming adiabaticity ($p \propto n^{\gamma}$) and taking $\gamma = 5/3$ leads to $n \propto I^3$ and $a \propto I^{-3/2}$.[13, 11, 7] A "sharp pinch" model[15] is typically assumed in which the plasma has radially uniform density and temperature contained within radius a, where the confining current exists in an infinitesimally thin layer. Then, the D-D fusion rate in the sharp pinch with deuterium density $n_D = n$ is

$$\dot{Y}_{DD} = \frac{1}{2} n^2 \langle \sigma v \rangle_{DD} \pi a^2 L, \tag{1}$$

where L is the plasma axial extent and $\langle \sigma v \rangle_{DD}$ is the Maxwellian-averaged D-D fusion reactivity, which scales approximately as $\langle \sigma v \rangle_{DD} \propto T^4$ from 1 to 10 keV.[16] (Notably, D-T reactivity also scales as $\propto T^4$ in the 1 to 10 keV temperature range.) The overall adiabatic scaling of D-D fusion yield rate is then $\dot{Y}_{DD} \propto I^{11}$ when assuming a constant linear density between equilibrium states.

Increasing the pinch current experimentally has demonstrated the corresponding increase in neutron yield, with DD yields $Y_n > 10^9$ neutrons per pulse in the FuZE-Q device, which was recently commissioned. The neutron

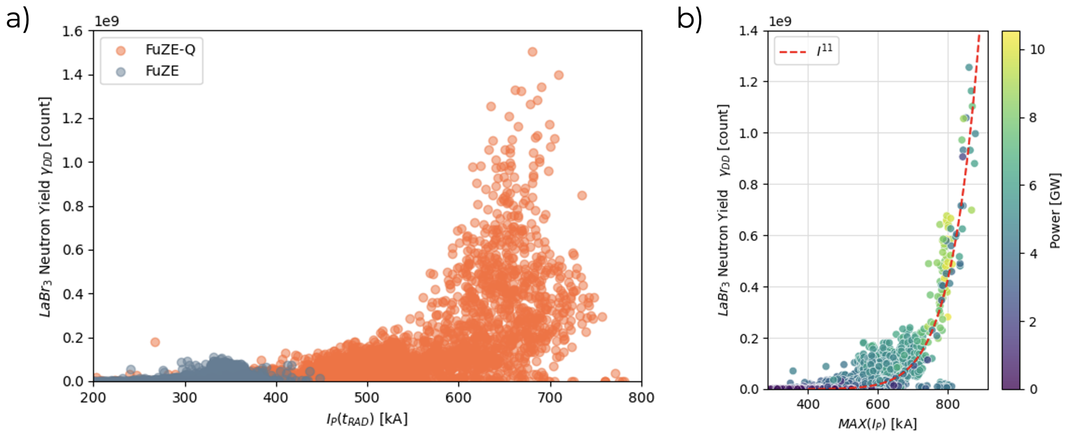

FIG. 6. a) The neutron yields as measured by LaBr activation detectors of all of the discharges taken on both the FuZE and FuZE-Q devices versus plasma current measured at peak neutron emission, labeled $I_p(t_{rad})$. b) A subset of FuZE-Q pulses taken from a controlled parameter scan, showing neutron yield scaling versus peak plasma current, MAX(I_p), matching the expected I^{11} from adiabatic compression.

yields of both the FuZE and FuZE-Q devices are shown in Fig. 6(a) versus plasma current. (In general, the expected scaling relationship exists versus the *pinch current* itself, not the total plasma current. However, the total plasma current offers a more reliable measurement from a Rogowski coil compared to the more complex method for deriving the pinch current from the surface magnetic field probe array in the assembly region. Heuristically, we have found that the total pinch current measured at the peak neutron emission time, $I_p(t_{rad})$, is a conservative proxy for the pinch current. This is the measurement that is used in these plots.)
Neutron yield scales strongly with plasma current on both devices, though the larger available stored energy on the FuZE-Q cap bank is able to generate pinches with significantly higher pinch currents. Figure. 6(a) consists of *all* pulses taken on both devices, without filtering for comparable pulse parameters. Figure 6(b) displays a subset of pulse for FuZE-Q taken with controlled parameter scan to study yield scaling versus current. The regression to this data set is consistent with $Y_n \propto I^{11}$ with an $R^2 = 0.74$, matching the expected I^{11} adiabatic scaling (see Ref. [6] for details). These new results show that when mass inventory and gas injection characteristics are properly coupled to the current waveform, the expected neutron scaling with plasma current is observed.

4. EFFECT OF IMPURITY CONTENT ON PERFORMANCE SCALING

4.1. Scientific Gain Q_{sci} with SFS Requirements

The scientific gain Q_{sci} of a SFS Z-pinch [17], is given by Eq. 2, where P_{fusion} is the DT thermonuclear fusion power, P_{th} is the thermal energy loss, P_{flow} is the flow power, P_{rad} is the radiative power loss, and P_α is the redeposited alpha power.

$$Q_{sci} = \frac{P_{fusion}}{P_{IN}} = \frac{P_{fusion}}{P_{th} + P_{flow} + P_{rad} - P_\alpha} \tag{2}$$

An equal population of deuterium and tritium is assumed, $n_D = n_T = n/2$ and that ion and electron temperatures are equilibrated, $T_e = T_i = T$.

$$P_{fusion} = \frac{n^2}{4} \langle \sigma v \rangle_{DT} E_{DT} V_p \tag{3}$$

$$P_{th} = \frac{3}{2}\left(1 + \bar{Z}\right) \frac{nT}{\tau_E} V_p \tag{4}$$

$$P_{flow} = \frac{1}{4}\left(m_D + m_T\right) \frac{n v_z^2}{\tau_{flow}} V_p \tag{5}$$

$$P_{rad} = C_B Z_{eff} \bar{Z}^2 n^2 T^{\frac{1}{2}} V_p \tag{6}$$

$$P_\alpha = f_c P_{fusion} \tag{7}$$

Note $E_{DT} \approx 17.6$ MeV is the energy yield per fusion event and the fusing plasma volume $V_p = \pi a^2 L_p$ where a is the pinch radius and L_p is the pinch length. The form of the radiative power loss P_{rad} assumes that Bremsstrahlung is the dominate loss mechanism, which is expected at the desired high gain operating points.

Next, the Alfvén speed at $r = a^+$ is given by Eq. 8 in the "sharp-pinch" limit, immediately outside of the surface current at r = a in this model.

$$v_A(a) = \frac{B_\theta(a)}{\sqrt{\mu_0 \rho}} \approx \frac{B_\theta(a)}{\sqrt{\mu_0 n m_i}} \tag{8}$$

Using the Bennett relation given by Eq. 9 it is clear the Alfvén speed scales with the sound speed, given by Eq. 10.

$$\beta = \frac{2\mu_o \langle p \rangle}{B_\theta^2(a)} = \frac{2\mu_o \left(1+\bar{Z}\right) nT}{B_\theta^2(a)} = 1 \tag{9}$$

$$c_s = \sqrt{\frac{2T}{m_i}} = \frac{v_A(a)}{\sqrt{1+\bar{Z}}} \tag{10}$$

The importance of this relationship is accentuated within the context of SFS, which requires a sufficiently large radially sheared axial flow to mitigate the growth of virulent plasma instabilities [7, 11, 13]. The required flow speed for stabilization can be expressed as Eq. 11, assuming a linearly varying flow within $r \in (0, a)$ and a coefficient $C_m \in (0.1, 0.5)$ from both linear and nonlinear stability theory [12].

$$v_z(a) \geq C_m k a v_A(a) = C_m k a c_s \sqrt{1+\bar{Z}} \tag{11}$$

Saturating the inequality in Eq. 11 and substituting into the subcomponents of Q_{sci} as applicable, the scientific gain Q_{sci} is given by Eq. 12. Note that though fusing plasma volume $V_p = \pi a^2 L_p$ is common to all terms, there is an explicit dependence on the pinch length L_p used to define the flow through time $\tau_{flow} = \frac{L_p}{v_z}$ and correspondingly the energy confinement time $\tau_E \approx \tau_{flow}$ as done previously [17].

$$Q_{sci} = \frac{\langle \sigma v \rangle_{DT} E_{DT}}{6\left(1+\bar{Z}\right)^{\frac{3}{2}} \frac{T}{nL_p} C_m c_s + \left(m_D + m_T\right) \frac{\left(C_m c_s \sqrt{1+\bar{Z}}\right)^3}{nL_p} + 4 C_B Z_{eff} \bar{Z}^2 T^{\frac{1}{2}} - f_c \langle \sigma v \rangle_{DT} E_{DT}} \tag{12}$$

4.2. Scaling to fusion conditions with impurities

A pinch length of $L_p = 0.5$ m is used in this analysis, motivated by the length of the compression region on the FuZE and FuZE-Q devices. Plasma operating contours (POPCon) are provided in Fig. 7 for various cases of Z_{eff} and f_c. The canonical case of $v_Z = 0.1 v_A$ and $\bar{Z} = Z_{eff} = 1$ with a chosen adiabatic trajectory are plotted in Fig. 7(a) and (b), indicating scientific breakeven $Q_{sci} = 1$ with a pinch current of approximately 650 kA. Higher flow speed requirements, such as a limiting $v_z = 0.5 v_A$, would lead to larger required plasma pressures to reach a desired triple product $p\tau_E$ because of shorter flow through times $\tau_{flow} \approx \tau_E$.

To compare to this pure hydrogenic case, an extreme case with impurities that limits the accessible $Q_{sci} \approx 10$ at a maximum pinch current $I_{pinch} = 2$ MA is given in Fig. 7(c) and (d), with $Z_{eff} = 4$ and $\bar{Z} = 2$. This limiting example is an extreme case, and would constitute a 20% fully ionized carbon impurity in the otherwise deuterium. Even so, this scaling is given to demonstrate that a reactor relevant design point with Q_{sci} is still possible even with significant impurity populations, but demanding higher density, temperature, and pinch current.

Additionally, redeposited alpha power can provide significant assistance in attaining high gains once entering the burning plasma regime $Q_{sci} \approx 5$ by reducing the required input power to balance both thermal and radiative losses. The same limiting case with $Z_{eff} = 4$ is considered but with half of the generated alpha power being deposited into the plasma (i.e., $f_c = 0.1$ in Eq. 12), as shown in Fig. 7(e) and (f). As expected, the scaling of the scientific gain is largely unchanged through breakeven, but then begins to diverge once alpha heating becomes a more dominate term in power balance. This assumed redeposition provides access to high gains $Q_{sci} > 10$ with pinch currents below 1.5 MA and temperatures below 20 keV. Thus, redeposited alpha power tends to improve the tolerance of this concept to high impurity content by reducing the required input power to compensate for the increased radiative and thermal losses when compared to the canonical hydrogenic case given in Fig. 7(a) and (b).

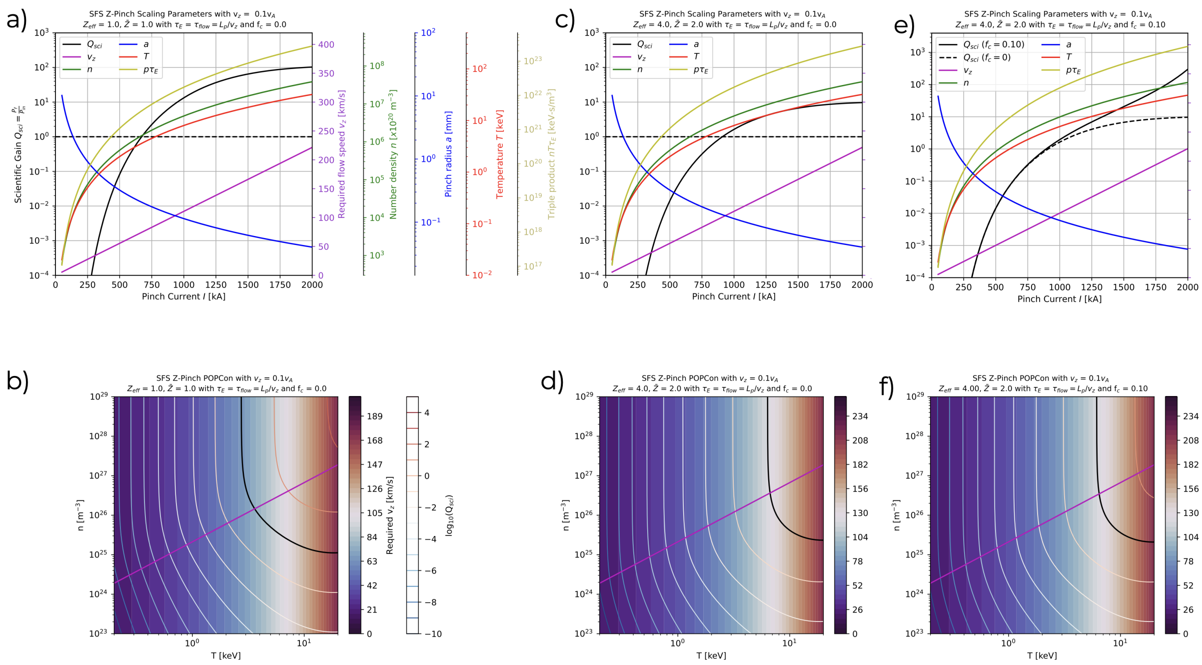

FIG. 7. Projected scaling plots and POPCons for various Z_{eff} and f_c. The top row shows parameter scalings as a function of pinch current for three cases; the bottom row shows associated POPCon for each case with adiabats shown in magenta. a) $Z_{eff} = \bar{Z} = 1$, with a chosen adiabat that predicts scientific breakeven at $I \approx 650$ kA. Note that power plant relevant $Q_{sci} \approx 10$ is predicted before reaching 1 MA with a reasonably high density plasma (i.e., mid-10^{26} m^{-3}). b) POPCon for case (a). Note the requirement for a minimum density $n \approx 1.5 \times 10^{25}$ m^{-3} to reach scientific breakeven even with temperatures up to 20 keV. c) $Z_{eff} = 4$, with a chosen adiabat that predicts scientific breakeven at $I \approx 900$ kA. Note that power plant relevant $Q_{sci} \approx 10$ is predicted at 2 MA, but requires very high density (i.e., $\approx 3 \times 10^{27}$ m^{-3}). d) POPCon for case (c). Note that $Q_{sci} = 10$ demands plasma temperatures in excess of 20 keV in this limiting example that would constitute a 20% fully ionized carbon impurity content. e) $Z_{eff} = 4$ with $f_c = 0.1$, i.e. half of the alpha power redeposited into the plasma. Note the significantly higher gains accessible in the burning plasma regime when compared to cases without alpha heating. f) POPCon for case (e). Projected scaling showing high gain is accessible for plasmas with temperatures below 20 keV, but still at quite high densities.

5. CONCLUSION

The FuZE-Q device, along with its newly commissioned 1 MJ class current driver, is predicted to be able to generate Z-pinch discharges characterized by triple products meeting Lawson criterion. Assuming continued performance scaling as shown here, the SFS Z pinch would make a compact fusion power plant. The simplicity of the device, enabled by its lack of need for external magnetic confinement, allows for a robust and economical plant design. A fusion power plant based on the SFS Z pinch has strong advantages over other approaches in a variety of aspects including size, cost, simplicity, and safety.

Here we support these efforts with updates from the FuZE and FuZE-Q machines. Elevated electron temperature, neutron yields consistent with adiabatic scaling and an extended axial pinch volume, as well as a performance robustness to Z_{eff} are steps to achieving the larger goal. As next efforts come online, including further advancements on our current drivers and upgrades to both FuZE and FuZE-Q, continued progress is anticipated.

ACKNOWLEDGEMENTS

The information, data, or work presented herein was funded in part by the Advanced Research Projects Agency – Energy (ARPA-E), U.S. Department of Energy, under Award Nos. DE-AR-0000571, DE-AR-0001010, DE-AR-0001260 and by the Air Force Office of Scientific Research under Grant No. FA9550-15-1-0271. This research used resources of the National Energy Research Scientific Computing Center (NERSC), a U.S. Department of Energy Office of Science User Facility located at Lawrence Berkeley National Laboratory, operated under Contract No. DE-AC02-05CH11231. Prepared by LLNL under Contract DE-AC52-07NA27344, LLNL-PROC-854534.

REFERENCES

[1] BANASEK, J. T., Probing local electron temperature and density inside a sheared flow stabilized Z-pinch using portable optical Thomson scattering, Rev. Sci. Instrum. **94** (2023) 023508.

[2] LEVITT, B. et al., Elevated electron temperature coincident with observed fusion reactions in a sheared-flow-stabilized Z pinch, submitted.

[3] MITRANI, J. M. et al., Measurements of temporally- and spatially-resolved neutron production in a sheared-flow stabilized Z-pinch, Nuclear Instruments and Methods in Physics Research Section A: Accelerators, Spectrometers, Detectors and Associated Equipment **947** (2019) 162764.

[4] MITRANI, J. M. et al., Thermonuclear neutron emission from a sheared-flow stabilized Z-pinch, Physics of Plasmas **28** (2021) 112509.

[5] THOMPSON, M. C. et al., Engineering paradigms for sheared-flow-stabilized z-pinch fusion energy, Fusion Science and Technology (2023).

[6] LEVITT, B. et al., The zap energy approach to commercial fusion, Physics of Plasmas **30** (2023).

[7] SHUMLAK, U. et al., Increasing plasma parameters using sheared flow stabilization of a Z-pinch, Physics of Plasmas **24** (2017) 055702.

[8] SHUMLAK, U. and HARTMAN, C. W., Sheared flow stabilization of the m=1 kink mode in Z pinches, Phys. Rev. Lett. **75** (1995) 3285–3288.

[9] SHUMLAK, U. et al., Evidence of stabilization in the Z pinch, Physical Review Letters **87** (2001) 205005.

[10] SHUMLAK, U. et al., Sheared flow stabilization experiments in the ZaP flow Z pinch, Physics of Plasmas **10** (2003) 1683–1690.

[11] SHUMLAK, U. et al., The sheared-flow stabilized Z-pinch, Fusion Sci. and Technol. **61** (2012) 119–124.

[12] MEIER, E. T. and SHUMLAK, U., Development of five-moment two-fluid modeling for Z-pinch physics, Physics of Plasmas **28** (2021) 092512.

[13] SHUMLAK, U., Z-pinch fusion, Journal of Applied Physics **127** (2020) 200901.

[14] BENNETT, W. H., Magnetically Self-Focussing Streams, Phys. Rev. **45** (1934) 890.

[15] BITTENCOURT, J. A., Fundamentals of Plasma Physics, 3rd Ed., Springer 2004.

[16] BOSCH, H. S. and HALE, G. M., Improved formulas for fusion cross-sections and thermal reactivities, Nuclear Fusion **32** (1992) 611–631.

[17] SHUMLAK, U., MEIER, E. T., and LEVITT, B. J., Fusion gain and triple product for the sheared-flow-stabilized Z pinch, Fusion Science and Technology **0** (2023) 1–16.